Allosteric Intermediates in Hemoglobin. 2. Kinetic Modeling of HbCO Photolysis[†,‡]

Robert A. Goldbeck,* Sarah J. Paquette, Sofie C. Björling,[§] and David S. Kliger

Department of Chemistry and Biochemistry, University of California at Santa Cruz, Santa Cruz, California 95064

Received September 19, 1995; Revised Manuscript Received February 27, 1996[⊗]

ABSTRACT: Nanosecond absorption spectra are measured in the Soret and near-UV spectral regions of human hemoglobin (Hb) after laser photolysis of the carbonyl adduct in order to study the dynamics of globin tertiary and quaternary conformational changes. Spectra and concentrations of physical intermediates, distinguished by extent of heme ligation and intraprotein relaxation, are obtained from a global analysis using a microscopic kinetic model that explicitly accounts for six observed relaxation and recombination processes. Three observed rate constants for CO rebinding and two intraprotein relaxation constants obtained are similar to constants determined by Hofrichter et al. [(1983) *Proc. Natl. Acad. Sci. U.S.A. 80,* 2235], the latter two comprising the 20−30-μs R → T quaternary transition and a previously unassigned 1-μs intraprotein relaxation. On the basis of the modeled intermediate spectra, as well as UV circular dichroism results observed on this time scale [Björling, S. C., Goldbeck, R. A., Paquette, S. J., Milder, S. J., & Kliger, D. S. (1996) *Biochemistry 35*, 8619−8627], the 1-μs relaxation is assigned to heme conformational changes concomitant with a relaxation of protein conformation at the $\alpha_1\beta_2$ interface corresponding to an initial step in a compound R → T reaction path.

The quaternary structural transition in human hemoglobin (Hb)[1] provides a mechanism for efficient physiological transport and regulation of dioxygen that is also of general interest as a model for the allosteric control of catalytic activity in enzymes. Despite extensive equilibrium and kinetic studies of the oxy and deoxy forms of hemoglobin, aided by knowledge of the X-ray crystal structures (Perutz, 1970; Baldwin & Chothia, 1979b), understanding of the microscopic mechanism for the interconversion of the quaternary structures remains incomplete. In particular, an open question is whether a concerted or compound mechanism operates (or indeed whether the complexity of the intraprotein forces in Hb blurs the classical distinction between these two limits). Along these lines, it has been suggested that unusual quaternary structures observed in some crystal forms of Hb may represent kinetic intermediates between stable oxy and deoxy structures (Doyle et al., 1992; Srinivasan & Rose, 1994). In the present paper and a companion article (Björling et al., 1996), we present time-resolved UV−visible spectral evidence for the existence of a metastable kinetic intermediate in the allosteric transition of hemoglobin after photodissociation of the carbonmonoxy complex.

Investigations of cooperative ligand binding in hemoglobin, using techniques such as X-ray crystallography (Baldwin & Chothea, 1979b), NMR (Ho, 1992), and absorption and circular dichroism (CD) spectroscopies (Perutz et al., 1974a; Bellelli & Brunori, 1994), have provided a wealth of information that has led to general acceptance of a two state model. In the two-state model of Monod, Wyman, and Changeux (MWC), the quaternary states of Hb comprise high-affinity, R, and low-affinity, T, conformers (Monod et al., 1965). The relative stabilities of the quaternary states are ligation dependent; addition of two or three ligands to the T state deoxy form causes the relative orientation of the $\alpha_1\beta_1$ and $\alpha_2\beta_2$ dimers making up the Hb tetramer to shift to the R conformation. The change in dimer−dimer geometry marking the T → R transition reduces dimer−dimer binding interactions at the $\alpha_1\beta_2$ interfaces (a reduction that is paid for with heme-ligand binding energy) and relaxes the global constraint on heme tertiary structure enforcing the lower ligand affinity of the deoxy form. The rate constants underlying the two-state MWC equilibrium model are summarized in Figure 1.

The positive feedback between ligand binding and affinity illustrated in Figure 1 makes intermediate ligation states difficult to study in hemoglobin, as equilibrium mixtures tend to be dominated by unliganded deoxy (T_0) or fully liganded oxy Hb (R_4). However, it is the character of ligand binding in the intermediate ligation states that most clearly distinguishes various models for Hb cooperativity, which range from the strictly concerted model of MWC to the purely sequential model of Koshland et al. (1996) (KNF). Whereas the classic MWC model maintained symmetry between subunits, it is now well established that subunit tertiary

[†] Financial support for this work was provided by the National Institute of General Medical Sciences (NIH), Grants GM-35158 and GM-38549.

[‡] This article is dedicated to the memory of our friend and colleague, Dr. Steven J. Milder.

* Author to whom correspondence should be addressed.

[§] Present address: Department of Medical Biophysics, MBB, Karolinska Institute, S-171 77 Stockholm, Sweden.

[⊗] Abstract published in *Advance ACS Abstracts,* June 15, 1996.

[1] Abbreviations: A_{576}, absorption at 576 nm; CD, circular dichroism; ΔOD, optical density of photolyzed sample minus optical density of prephotolysis sample; DI, deionized; Hb, human hemoglobin A; Mb, myoglobin; NMR, nuclear magnetic resonance; ns, nanosecond; OD, optical density; OMA, optical multichannel analyzer; R, (relaxed) quaternary structure of liganded hemoglobin; *r*, tertiary structure of liganded subunit; S/N, signal to noise ratio; SVD, singular value decomposition; T, (tense) quaternary structure of unliganded hemoglobin; *t*, tertiary structure of unliganded subunit; TRCD, time-resolved circular dichroism; TROD, time-resolved optical density; UV, ultraviolet.

S0006-2960(95)02248-3 CCC: $12.00

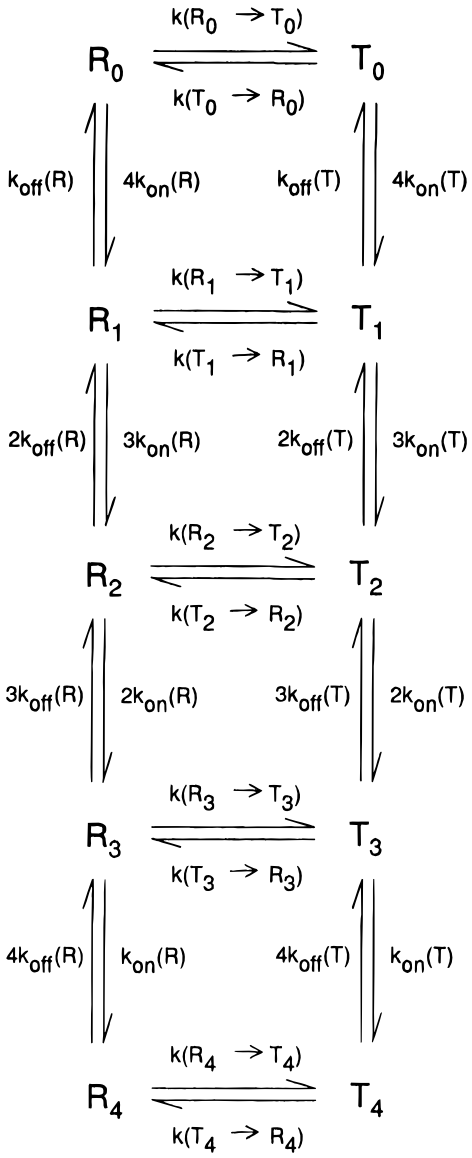

FIGURE 1: Two-state model of Hb cooperativity showing the forward and backward rate constants for equilibria connecting the ten species distinguished by quaternary state, T and R, and extent of heme ligation (subscripts). The rate constants for CO binding, k_{on} and k_{off}, are postulated to depend on quaternary state, independently of ligation. If the ratio of T and R affinities is designated as c, then the allosteric equilibrium constants, L_i, are related by $L_i = [T_i]/[R_i] = Lc^i$, where $L = L_0 = k(R_0 \rightarrow T_0)/k(T_0 \rightarrow R_0)$. A value of $L = 9000$ is obtained by Matsukawa et al. (1981) for human Hb A at 25 °C, pH 7, and a value of $c = 0.004$ typifies CO binding under these conditions (Jameson & Ibers, 1994).

structure is directly altered by ligand binding ($t \rightarrow r$) (Shulman et al., 1975; Brzozowski et al., 1984), and this feature has been incorporated into hybrids of the MWC and KNF models in which the perturbation of subunit tertiary structure imposed by ligand binding is coupled to the position of the two-state quaternary equilibrium mediating heme−heme communication (Perutz, 1970; Herzfield & Stanley, 1974; Lee & Karplus, 1983; Ackers et al., 1992). Ackers and co-workers (1992) have characterized the thermodynamics of ligand binding and dimer−dimer binding in intermediate ligation states and conclude that the coupling of tertiary structure and quaternary equilibrium exhibits the following symmetry rule: The quaternary structure switches from T to R whenever both dimers have at least one ligand, i.e., the acquisition of an *r* subunit in both dimers is the pivotal event triggering the global shift in protein structure. They further find evidence for sequential cooperativity within the R and T quaternary forms, but this point is more controversial, with the strongest negative evidence coming from ligand binding measurements in hemoglobins lacking a quaternary transition because of chemical modifications, mutations (Imai, 1982), or crystal packing constraints (Mozzarelli et al., 1991). Thus, it is not clear whether significant intersubunit communication takes place independently of the global transition between T and R.

The binding of ligands such as oxygen and carbon monoxide to hemoglobin is a dynamic process, and thus additional information about the mechanism of Hb cooperativity has come from time-resolved spectral measurements after ligand photolysis (Bellelli & Brunori, 1994). Despite the elusiveness of intermediate ligation states in equilibrium studies, species such as R_0, R_1, R_2, and R_3 can be readily generated and studied by the photolysis of photolabile ligands such as CO. The present study examines Hb under conditions of high CO saturation and high photolysis (90% photolysis yield) that are known to produce switching of globin quaternary conformation in a portion of tetramers representing about 30% of the deligated hemes remaining after geminate recombination (Hofrichter et al., 1983, 1991; Jones et al., 1992). Time-resolved absorption data focusing on the kinetics associated with quaternary state switching is analyzed in this paper in the context of a microscopic model that is consistent with the two-step picture of the R → T transition advanced in the preceding paper in this issue (Björling et al., 1996). In particular, the signal-to-noise ratio of the absorption data permits us to measure the time constant of the small amplitude process near 1 μs, elusive in previous studies and implicated by time-resolved circular dichroism (preceding paper) and resonance Raman evidence (Jayaraman et al., 1995) in the quaternary transformation, with good reliability.

Several questions are addressed by the kinetic modeling of multichannel Soret band absorption data presented below. First, it is of interest to know whether the current, phenomenological understanding of HbCO photolysis spectrokinetics in terms of observed time constants and their associated spectra (b-spectra) can be successfully translated into a microscopic kinetic model, albeit a simplified one. Even a simplified model represents an advance in that it demonstrates that, in the absence of complete knowledge of the kinetic mechanism in Hb, a perturbative approach using reasonable approximations can yield useful information about the spectrokinetic properties of the allosteric intermediates. Kinetic modeling is required to obtain the microscopic rate constant for the $R_0 \rightarrow T_0$ transition observed at about 20 μs, for instance, as the observed time constant for this process is expected to be influenced by concurrent CO recombination. It is through such microscopic allosteric rate constants that a quantitative connection can eventually be made between kinetics and the large body of equilibrium data for the thermodynamics of Hb allostery. Finally, and potentially of most significance for the present work, we can ask: what information about the physical nature of the intermediates is revealed by their microscopically modeled spectra? In this regard, we point out that the modeled intermediate spectra are expected to be more useful guides than phenomenological basis spectra, such as those produced by singular value decomposition or global fitting to simple exponential

decays, which are mixtures of the physical intermediate spectra. In particular, we find from this analysis that the modeled absorption difference spectrum characterizing the 1-μs relaxation process preceding the 20-μs quaternary transition closely resembles the equilibrium T − R difference spectrum, in agreement with the evidence presented in the preceding paper that this process corresponds to the first step in a compound R → T transition.

MATERIALS AND METHODS

Sample Preparation. Native human Hb, free of membrane and other low molecular weight components, was prepared in the oxy form from fresh blood from a nonsmoking donor using published procedures (Geraci et al., 1969). Washing with 1% NaCl solution followed by centrifugation at 4000*g* was repeated four times before lysis with DI water and centrifugation at 10 000*g*. The supernatant was dialyzed over a 48-h period against 0.1 M sodium phosphate buffer. Beads of concentrated oxyHb were prepared by suspending small droplets of the (non-stripped) protein into liquid nitrogen. OxyHb beads were redissolved for use and diluted to a final concentration of 120 μM in heme (dimerization < 10%), based on literature extinction coefficients at 570 nm (Antonini & Brunori, 1971), in a CO-flushed, 0.1 M, pH 7.3, sodium phosphate buffer prepared from Millipore-filtered water. Equilibration with gases (N_2, CO) and static spectrophotometric measurements were done at room temperature. An optical density of approximately 1 was obtained for HbCO in both spectral regions with a 2-mm path length cell in the UV and a 0.5-mm path length cell in the Soret. A carbon monoxide pressure of 1 atm (water-saturated CO) was applied to the solutions for 1 h to assure complete formation of the carbonyl complex. Samples were then introduced into a CO-flushed oxygen-free sample reservoir and allowed to equilibrate in the apparatus for one-half hour to ensure a final solution concentration of ∼1.0 mM free CO. Full reduction to ferrous heme was obtained by anaerobic injection of fresh sodium dithionite solution into the sample with a Hamilton air-tight syringe for a delivered concentration of 540 μM. Both the absorbance changes upon addition of reductant to the sample and the ratios of final absorbances, A_{576}/A_{560} and A_{540}/A_{560}, indicated that only very small amounts of methemoglobin or the oxy-derivative remained. The permanent bleaching of sample after multiple flashes during an experimental run was minimized by flowing a large volume of sample. A small Teflon stopcock controlled the gravity flow of a 40 mL aliquot of sample from an upper reservoir, through the cell, into the bottom reservoir. After obtaining a set of measurements on a sample, the sample was recycled for a second set of measurements by applying the force of the inlet CO pressure to return the sample to the top reservoir. Reversibility was tested by comparing decarboxylation and recarboxylation absorbances. Sample integrity was demonstrated by the similarity of photolysis spectra for the 16-ns probe time obtained from the two experimental runs, and by the comparable ultraviolet visible (UV−vis) spectra recorded from 185 to 650 nm.

Spectral Measurements. Static absolute and difference spectra for HbCO and deoxy-Hb were measured with a UV−vis spectrophotometer interfaced to a computer for analysis and processing. The nanosecond absorbance spectra were measured on a laser photolysis apparatus described previously (Lewis et al., 1987). HbCO was photolyzed by 7-ns, 15-mJ pulses of the 532-nm second harmonic from a Nd:YAG laser. The temperature of the photolysis sample cell was maintained at 20 °C with a recirculating water bath. Transient events were monitored by a pulsed xenon flashlamp and a time-gated optical multichannel analyzer (OMA), the time gate provided by 10-ns pulses from a pulse amplifier. A spectrograph dispersed light from the flashlamp with a spectral resolution of approximately 2 nm using an entrance slit width of 100 μm. A model 1420QB OMA detector (EG&G, Princeton, NJ) was used for the near-UV optical density measurements, and a model 1420R detector (EG&G) was used in the Soret.

The actinic pulse entered the sample nearly collinear with the probe beam. Linear dichroism measurements showed the presence of photoselection effects up to 36 ns after excitation with the linearly polarized laser (data not shown); therefore, the polarization of the probe beam was set to magic angle (54.7°) relative to the vertically polarized actinic beam to eliminate kinetic artifacts due to rotational relaxation.

Measurements were taken at logarithmic delay times from zero time (defined by the time of maximum laser scatter), with 10 points in each time decade from 16 ns to 200 ms. The data thus collected consisted of an array of transmitted intensities, indexed by wavelength and time, for both the photolyzed and unphotolyzed sample, with each column representing the average of 16 spectral measurements (after subtraction of a dark count correction). Photolysis difference spectra were calculated at each delay time as the log of the ratio of the intensity columns for photolyzed and unphotolyzed HbCO. Twelve such sets of measurements were collected in the Soret and averaged together and three in the near-UV, thereby improving the signal to noise ratio in each spectral region by factors of 15 and 10, respectively, compared with a single OMA absorption measurement. The OMA detector acquires about 720 optical absorption data points at 0.6-nm intervals during each spectral measurement. The number of wavelengths was reduced to 112 in the Soret and 149 in the near-UV by retaining only wavelengths between 405 and 470 nm in the Soret and between 250 and 335 nm in the near-UV.

Singular Value Decomposition. The global fitting of multiple exponential relaxations to large data arrays (112 × 64 in the Soret and 149 × 62 for the UV) is made more efficient by the use of singular value decomposition (SVD) (Eckhart & Young, 1939; Hendler & Shrager, 1994). The SVD algorithm decomposes the data array into a matrix product that may be truncated to retain only the most significant spectral and temporal features of the data (Henry & Hofrichter, 1991; Goldbeck & Kliger, 1993).

The $m \times n$ data matrix **A**, containing spectral data for m wavelengths and n time delays after photolysis, can be decomposed as the product of three matrices

$$\mathbf{A} = \mathbf{USV}^{\mathrm{T}} \tag{1}$$

where the $m \times n$ matrices **U** and **V** both consist of columns of orthonormal vectors ($\mathbf{V}^{\mathrm{T}}$ is the transpose of **V**), and **S** is an $n \times n$ diagonal matrix. The diagonal elements of **S** contain the non-negative singular values of **A** arranged in order of decreasing value. The columns of **V** form an orthonormal basis set of time courses that are related by a linear transformation (not specified by the SVD) to the

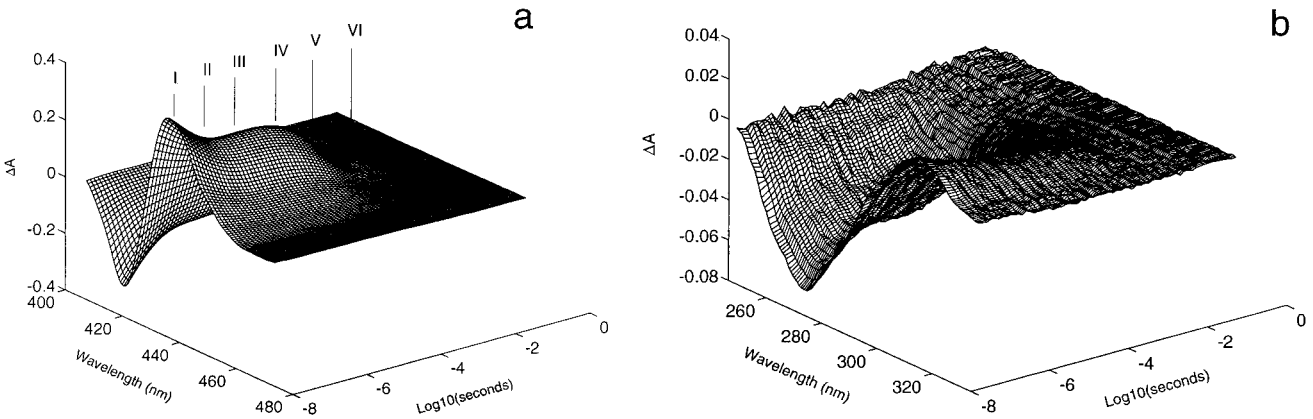

FIGURE 2: Time-resolved absorption of HbCO after photolysis at 20 °C, pH 7.3. Photolysis difference spectra for the (a) Soret and (b) near-UV spectral regions. Relaxation phases I−VI are shown in panel a.

temporal evolution of the concentrations of physical intermediates. Similarly, the columns of **U** constitute an orthonormal set of basis spectra from which the spectra of the physical intermediates contributing to **A** may be determined given the transformation connecting the time course bases and the intermediate concentrations. The form of eq 1 shows that the contribution of the product of a particular basis spectrum and its time course to the data in **A** weighted by the corresponding singular value. Since smaller singular values will correspond mostly to the contribution of random noise to the array **A**, it is useful to truncate **S** at the element *s* containing the smallest singular value that can be distinguished from noise and discard the SVD decomposition for the remaining singular values. The index *s* is the effective rank of the matrix. The resulting data representation $\mathbf{A}_s$, i.e., the matrix product of the first *s* columns of **U**, the $s \times s$ upper left hand of **S**, and the first *s* rows of $\mathbf{V}^T$, is the best least-squares approximation to **A** in the sense that the sum of squares of the differences between the elements of **A** and $\mathbf{A}_s$ is given by summing the squares of the discarded singular values (Henry & Hofrichter, 1991).

Kinetic Analysis. The truncated data representation is used as input for the global exponential fitting process, which employs a simplex algorithm to obtain apparent lifetimes for the kinetic intermediates by simultaneously fitting the time amplitudes of the significant spectral components to a set of exponential relaxations. Analyses were performed on a workstation using Matlab software (The Math Works).

The global kinetic fitting of the truncated data representation can be written as

$$\mathbf{A}_s = \mathbf{B}\mathbf{T}^T \tag{2}$$

where the columns of the $m \times k$ matrix **B** contain the spectra of *k* intermediates and the columns of the $n \times k$ matrix **T** contain their concentrations as a function of time. Use of eq 1 for $\mathbf{A}_s$ in eq 2 shows that the (truncated) matrix of time bases can be related to the time evolution of the intermediates by a transformation matrix **D**,

$$\mathbf{V}_s^T = \mathbf{D}\mathbf{T}^T \tag{3}$$

where $\mathbf{D} \equiv \mathbf{S}_s^{-1}\mathbf{U}_s^T\mathbf{B}$. The spectra of the intermediates are then found from

$$\mathbf{B} = \mathbf{U}_s\mathbf{S}_s\mathbf{D} \tag{4}$$

Global kinetic fitting consists of varying the parameters of **T** and the $s \times k$ elements of **D** to minimize the sum of squares of the differences between matrix elements of $\mathbf{V}_s^T$ and $\mathbf{D}\mathbf{T}^T$, with each row weighted by its singular value.

RESULTS

Time Evolution of the Photolysis Difference Spectrum. The time evolutions of hemoglobin photointermediate absorption difference spectra are shown as surface plots in Figures 2a and b for the Soret and near-UV spectral windows, respectively. The Soret measurements span the time interval from 16 ns to 90 ms after photolysis; the near-UV measurements end at 50 ms. A point on each surface represents the average of several hundred absorbance measurements. Signal averaging reduces the random noise content of the data to a nearly imperceptible level in Figure 2a (peak S/N $\approx$ 1000). The smaller magnitude of the photolysis difference spectrum in the near-UV is responsible for the lower S/N evident in Figure 2b (peak S/N $\approx$ 100). Overall, the low noise content and the large number of data points collected ($N \approx 10^4$) give the data a very high statistical power in the global fitting of parameters presented below.

The return to equilibrium HbCO after ligand photodissociation shown in Figure 2 is multiphasic. An initial phase combining geminate CO recombination (relaxation I) and intraprotein relaxation (II) precedes a plateau at around 1 μs (III). This plateau is followed by fast (V) and slow (VI) second-order rebinding phases with pseudo-first-order time constants of ca. 200 μs and 4 ms (1 atm of CO), respectively. This is in contrast to myoglobin−CO photolysis, in which a very brief geminate rebinding phase is followed by a single diffusive rebinding phase with a lifetime of about 1.8 ms. The fast and slow diffusive rebinding species in Hb correspond to the R and T allosteric states, a distinction that cannot arise in noncooperative Mb. The conversion of R_0 to T_0 (relaxation IV) competes with ligand rebinding to R_0.

The evolving isosbestic observed in Hb also contrasts with myoglobin. The earliest difference spectrum has a spectral signature that is red shifted from that of the static deliganded minus liganded difference spectra, with later difference spectra evolving toward the static difference spectrum. The lack of a fixed isosbestic indicates the presence of multiple, spectrally distinct intermediates arising between ligand photolysis and eventual recombination. At least some of the evolution after 10 μs must be attributed to the R $\rightarrow$ T transition known to take place on this time scale (Hofrichter et al., 1983). From the equilibrium T − R difference spectrum, this is expected to produce a small blue shift in

the Soret absorption band (Perutz et al., 1974a). After about 100 μs, however, ligand recombination competes with quaternary relaxation and extinguishes the spectral evolution associated with the latter process, as is evident in Figure 2a. Additional contributions in Figure 2 arising from spectral differences between different Hb ligation states due to heme−heme interactions cannot be ruled out, but there seems to be little evidence for such differences. The evolution seen at early times is presumably due to relaxation of tertiary structure near the photolyzed hemes. It has been suggested that increasing distance of the iron out of the heme plane is correlated with a blue shift in the Soret bands (Perutz et al., 1974b; Murray et al., 1988) so that constraints imposed by the tertiary and quaternary structure of the protein on heme relaxation, particularly on the N_ϵ−Fe bond distances, could account for the evolving isosbestic.

The SVD components are of interest primarily because they form a unique and compact representation of the data. Although we discuss the spectrokinetic features of particular physical processes contained within the SVD basis functions, it should be emphasized that the vectors of **U** (**V**) are mathematical constructs that mix the spectral (temporal) properties of physical intermediates in order to satisfy the constraint of orthogonality. A plot of the log of the singular values in their rank order typically reveals a break in slope between the largest values, corresponding to significant data, and the remaining values, corresponding to random noise. A plot of the Soret singular values (not shown) indicates that the first five values are significant, i.e., the data matrix is of effective rank 5. (Three or four values are significant in the near-UV.) The five most significant SVD components of the Soret data are displayed in Figure 3a−j. The basis spectra are plotted on the left, scaled by their singular values (columns of the matrix **US**), and the associated time courses (columns of **V**) are plotted on the right. Jones et al. (1992) report four SVD components for data obtained at 16 levels of photolysis, with two components regarded as significant within the signal to noise. The spectral components reported there are generally similar to the first four components shown in Figure 3, with the exception of artifactual differences noted below for the second and fourth spectral components.

The first basis spectrum is generally the best one-component least-squares fit to the original spectral data (Henry & Hofrichter, 1991). The first Soret basis spectrum, U_1 (U_1S_1 in Figure 3a), thus corresponds primarily to the deoxyCO difference spectrum and the corresponding time course, V_1 (Figure 3f), largely reflects the course of CO rebinding. A simple ligand rebinding curve generated by plotting loss of spectral intensity at the deoxy absorption wavelength vs the log of time (not shown) is in general agreement with V_1. However, an exponential analysis of V_1 shows the presence of rate processes corresponding to protein relaxations (relaxations II and IV in Table 1) in addition to recombination processes (I, V, and VI), and thus the spectral signatures for these relaxation processes are also convoluted into U_1. The spectral changes represented by the higher SVD components are much smaller. The second basis spectrum, U_2 (Figure 3b), shows spectral evolution in the deoxy hemes and contains information about changes in protein structure in the vicinity of the heme chromophore after photolysis. Indeed, it shares similarities with the equilibrium T − R spectral difference (Perutz et al., 1974a),

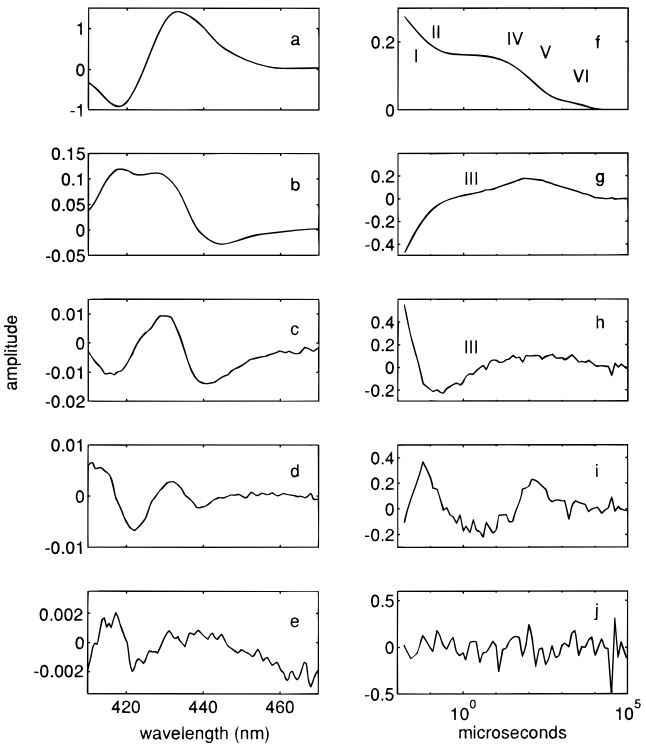

FIGURE 3: SVD basis spectra and time amplitudes for the data in Figure 2. The first five basis spectra (columns of **U** matrix) (panels a−e) and time amplitudes (columns of **V**) (panels f−j) for the Soret region.

Table 1: Time Constants Obtained from fit of Soret Band Data, 20 °C, pH 7.3, to Sum of Six Exponential Relaxations and Their Relative Amplitudes

	τ_1	τ_2	τ_3	τ_4	τ_5	τ_6
relaxation	I	II	III	IV	V	VI
Soret amplitude	22 ns 0.16	83 ns 0.29	1.3 μs 0.02	38 μs 0.11	180 μs 0.30	3.9 ms 0.11

having a zero crossing at 438 nm between a long wavelength minimum near 440 nm and short wavelength maximum near 430 nm. Correspondingly, V_2 (Figure 3g) shows an increase from zero amplitude near 1 μs to a maximum positive value near 100 μs that then decays with the T state recombination lifetime, the general profile expected for the T state contribution. The largest contribution to V_2, however, corresponds to geminate recombination. [The second maximum on the blue side of the carboxy peak, near 420 nm in U_2, is an artifact caused by stray light detection within the Soret band of the carboxy sample. This artifact appears to contribute only a small shoulder at similar locations in the U_2 basis spectra of Hofrichter et al. (1983) and Jones et al. (1992)]. The largest contribution to the third pair of basis vectors, U_3 and V_3, is also from geminate recombination, but a 1-μs process is prominent in V_3 along with a spectral feature resembling the T − R difference in U_3. The fourth pair of basis vectors apparently contains both deoxy spectral evolution and CO-ligation changes. It is very similar to the basis spectrum reported by Jones et al. (1992) after the base line dispersion artifact encountered in that study is taken into account. The fifth pair of components reported in Figure 3 is difficult to distinguish from noise.

Global Fit to Exponential Relaxations. The time course of the five most significant absorbance changes obtained from SVD in the Soret region were fit to sums of exponen-

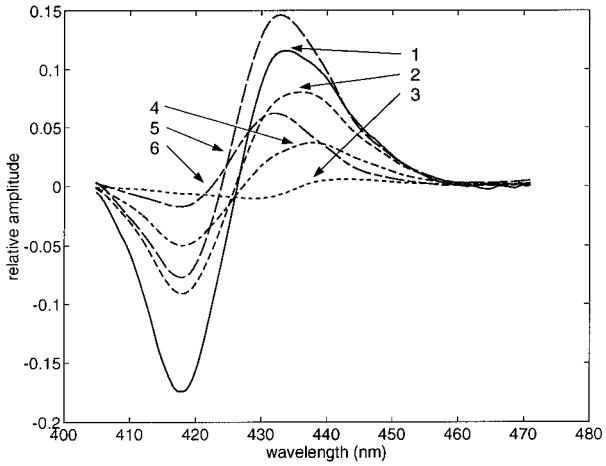

FIGURE 4: Absorbance changes (b-spectra) associated with the apparent lifetimes in a six-exponential fit for the Soret region: b_1 (—), b_2 (- - -), b_3 (•••), b_4 (-•-), b_5 (— — —), and b_6 (— - —).

tials. In this procedure, the sum of squares of the differences between the fit, with n rate constants, and the data points is minimized on the assumption that the rate constants are the same for all wavelengths, i.e., a global kinetic fit. This procedure then returns time constants and spectral changes (b-spectra) associated with each exponential relaxation. Time courses for the Soret region were fit by the non-linear global fitting procedure to six exponentials in the time range from 16 ns to 200 ms to give the set of apparent lifetimes displayed in Table 1 (lifetimes obtained from the near-UV data are very similar) and their spectral amplitudes (b-spectra) shown in Figure 4. The relative integrated spectral amplitudes associated with each of the apparent time constants are given in Table 1 as an indication of the relative contribution of each time constant to the overall spectral dynamics. Five of the time constants (τ_1 and τ_3−τ_6) are in general agreement with the 5-exponential results of Hofrichter et al. (1983). The addition of a sixth rate constant splits the 0.5−1-μs rate observed by Hofrichter et al. (1983) into two time constants of about 100 ns and 1 μs (τ_2 and τ_3). The addition of the 100-ns lifetime relaxation, relaxation II, in the exponential analysis of the time-resolved absorption data presented here results in a smaller amplitude and reduced uncertainty in measured lifetime for relaxation III and also shortens the measured lifetime for relaxation I, geminate recombination, over a five-exponential fit. Standard statistical tests of goodness of fit (χ_r^2 and F-test) support the significance of the additional parameters introduced by the six-exponential fit over a five-exponential fit. Further support for the significance of the additional lifetime is found in the reproducibility of the six-exponential fit among individual experimental trials (not shown) before averaging into the tabulated results. One feature of this reproducibility is a more stable fit for the 1-μs lifetime (τ_3) than is found in a five-exponential fit. Jones et al. (1992) report very similar lifetimes, 20, 90, and 820 ns for relaxations I, II, and III, respectively, for HbCO under similar photolysis conditions.

The Soret b-spectra (Figure 4) associated with the recombination processes (I, V, and VI) resemble the difference spectrum for unliganded−liganded heme, as does the b-spectrum for τ_2, although the spectrum for relaxation VI is blue shifted from I and V. The b-spectrum for relaxation III, on the other hand, resembles the ligation independent R − T difference spectrum of Perutz et al. (1974a). Spectrum

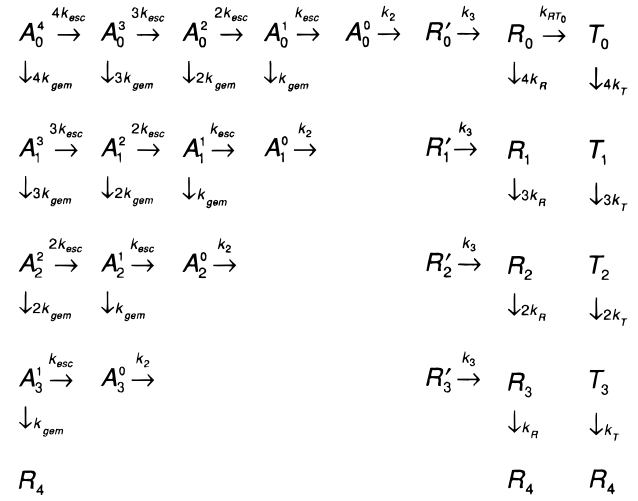

FIGURE 5: Kinetic model for photodissociation of Hb ligand complex accounting for three protein relaxations and geminate and second order ligand recombination. Superscripts indicate number of geminate pairs within an Hb tetramer, thus the species A_n^k contains k geminate pairs, corresponding to R_r'[Fe•••CO] in Scheme 1, and n ligated hemes. The rate constants for geminate recombination to a single heme in R state Hb and for ligand escape from the protein into the solvent are k_{gem} and k_{esc}, respectively. For $n < 4$, R_n' denotes photodissociated R state HbCO retaining the unrelaxed intersubunit conformation of equilibrium HbCO and R_n denotes a partial relaxation of intersubunit conformation. The model neglects $R_n \rightarrow T_n$ for $n > 0$, as well as any back reactions, and does not distinguish between recombination to α and β chains. Although 26 intermediates are distinguished, their spectra are not independent; the intermediate spectra are treated as composites of six independent spectra (see Figure 7).

IV appears to be a mixture of the unliganded−liganded difference and the R − T difference spectra.

Calculation of Difference Spectra of Photolysis Intermediates from Kinetic Modeling. We present here an analysis of the multichannel absorption spectroscopy of HbCO photolysis in the context of an explicit kinetic model. This model contains microscopic rate constants for physical processes underlying the observed rate constants obtained from simple exponential analyses. Although the model presented is certainly oversimplified, it enables the calculation of spectra and concentrations for important physical intermediates of interest. The intermediate spectra will in general be linear combinations of b-spectra, with the combination coefficients depending on details of the kinetic model. Elucidating the spectra of intermediates is useful in assigning their physicochemical nature, and thus represents an advance over b-spectra, which generally mix the properties of physical intermediates. However, an important caveat to the present analysis arises from the fact that the maximum amplitudes of the spectral changes described by the higher SVD components presented above are small compared to the maximum ΔOD, i.e., only small perturbations of the average deoxyCO difference spectrum occur between photolysis and recombination. Given the large number of intermediates that can be distinguished by ligation state and protein structural state in microscopic models of HbCO photolysis kinetics, the characterization of a complete kinetic mechanism involving such spectrally similar intermediates remains a challenge.

The model in Figure 5 accounts for three protein relaxations and geminate and second-order ligand recombination, beginning with the independent heme reaction steps shown

Table 2: Microscopic First-Order Rate Constants (s^{-1}) Obtained from Fit of Soret Photolysis Data to Kinetic Model (Lifetimes in Parentheses)

k_{gem}	k_{esc}	k_2	k_3	$k_{R_0 \rightarrow T_0}$	k_{R+CO}	k_{T+CO}
2.3×10^7 (53 ns)	4.2×10^7 (28 ns)	1.2×10^7 (91 ns)	1.3×10^6 (770 ns)	2.9×10^4 (38 μs)	6.4×10^3 (160 μs)	2.7×10^2 (3.7 ms)

Scheme 1

$$R_r[Fe-CO] \underset{k_{gem}}{\overset{h\nu}{\rightleftarrows}} R_r'[Fe\cdots CO] \overset{k_{esc}}{\underset{-CO}{\rightleftarrows}} R_r'[Fe-] \overset{k_2}{\rightarrow} R_t'[Fe-] \overset{k_3}{\rightarrow} R_t[\text{perturbed interface}]$$

I II III

in Scheme 1. Photodissociation of the Fe−CO bond produces the geminate pair [Fe···CO] within the R protein quaternary conformation and with the *r* tertiary configuration still unrelaxed at the photolyzed heme. The prime notation on R indicates that the quaternary conformation of the tetramer remains in the crystallographic R state of fully ligated Hb, before the conformation of the protein at the subunit interfaces relaxes to accommodate deligation. The geminate pair decays through ligand recombination (k_{gem}) and ligand escape from the protein into the solvent (k_{esc}). Deligated heme undergoes $r \rightarrow t$ tertiary relaxation (relaxation II) with rate constant k_2. Relaxation III (k_3) produces the species R, postulated to differ from the R′ structure by a protein structural relaxation affecting the $\alpha_1\beta_2$ interface. From microscopic reversibility, we identify R_0 with the traditional R_0 species in equilibrium with T_0, cf. Figure 1. Relaxation III is postulated to bring the system to the brink of cooperativity by setting the stage for the gross change in dimer−dimer orientation required to reach the T quaternary state. Ensuing steps in the overall kinetic model will then be influenced by heme−heme communication mediated by the R → T transformation.

The independent heme processes are incorporated into a kinetic model for the tetramer using combinatorial statistics for four hemes. [Although the roughly parallel orientation of the hemes within the tetramer can be expected to skew the distribution of photoproducts away from the statistical distribution that would be produced by randomly oriented hemes toward a preponderance of fully photodissociated tetramers, this biasing effect is found to be small (Hofrichter et al., 1991).] The partial photolysis of ligated tetramer produces a species with *m* geminate pairs and *n* unphotolyzed hemes, denoted as A_n^m in Figure 5. Statistically, there are 15 such species, including the starting material $A_4^0 = R_4$. Although their kinetics are independent of ligation except for the statistical factors appearing in the rates, these species must be distinguished in the model to properly account for formation of later intermediates whose kinetics depend on heme−heme interactions.

Relaxation IV involves the R → T transition and is expected to depend on the extent of tetramer ligation. Only the fastest quaternary transition, $R_0 \rightarrow T_0$, is included in the present model. Relaxation IV then corresponds to branching between $R_0 \rightarrow T_0$ and ligand recombination with R_0. The right hand side of Figure 5 corresponds to the two-state model in Figure 1 with all back reactions and $R_n \rightarrow T_n$, $n > 0$, steps removed (and buildup of T_4 neglected). Diffusive ligand recombination within R_{1-3} gives rise to the observed time constant for relaxation V, $\tau_5 = k_{on}(R)^{-1}$, and T_{0-3} + CO gives rise to the time constant for relaxation VI, $\tau_6 = k_{on}(T)^{-1}$. Kinetic differences between α and β chains are ignored, as is the effect of the small amount of dimers present. The model assumes that relaxation I reaches completion within a tetramer before relaxation II begins and that II is complete before III begins. Diffusive ligand recombination to intermediates preceding R is also neglected. An important simplification is also introduced during global modeling of the intermediate spectra: Although 26 intermediates are distinguished by the model, their spectra are not treated independently. The intermediate spectra are modeled as composites of six independent spectral functions, corresponding to six ligation/relaxation states possible at each heme. These are the geminate pair, unrelaxed pocket, relaxed pocket, R, unligated heme within T tetramer, and ligated heme within T tetramer.

Table 3: Observed Time Constants Obtained from Fit of Soret Photolysis Data to Kinetic Model

relaxation	I	II	III	IV	V	VI
	15 ns	83 ns	790 ns	18.2 μs	160 μs	3.7 ms

The kinetic matrix for *n* intermediates has *n* eigenvalues corresponding to as many observed rate constants, but in the present case many of the eigenvalues are degenerate or nearly degenerate. For this reason, the six observed rates obtained in the simple exponential analysis may be approximately identified with the observed rate constants for the 26 × 26 matrix. A further divergence from the simple exponential analysis comes with the addition of the constraint on spectral composition of the intermediates introduced above. This constraint changes the time constants giving the best fit to the data. Thus, in fitting the data to the kinetic model it was necessary to allow the microscopic rate constants associated with each process to vary from the values calculated from the time constants for the six-exponential fit.

The geminate yield for HbCO photolysis is $0.4 = k_{gem}/(k_{gem} + k_{esc}) = \phi$. The observed geminate yield was lowered to 0.3 by rephotolysis of geminately recombined complex during the finite length of the laser pulse. To account for this, the model was run in two steps. The first step explicitly included the photodissociation rate as a constant (not shown) in order to model the excitation as a step pulse. The excitation step was allowed to run for 15 ns, the time required to reduce the observed geminate yield according to the approximate relation $\phi_{obs} = \phi \exp\{-(1 - \phi)t/\tau_1\}$, where τ_1 is the observed lifetime of the geminate process. The intermediate populations obtained this way were then used as starting conditions for the second step, during which the photodissociation rate was turned off.

The microscopic rate constants obtained from fitting the model to the Soret absorption data are shown in Table 2. The approximate observed time constants calculated for relaxations I−VI shown in Table 3. The time evolutions of intermediate concentrations obtained from fitting of the

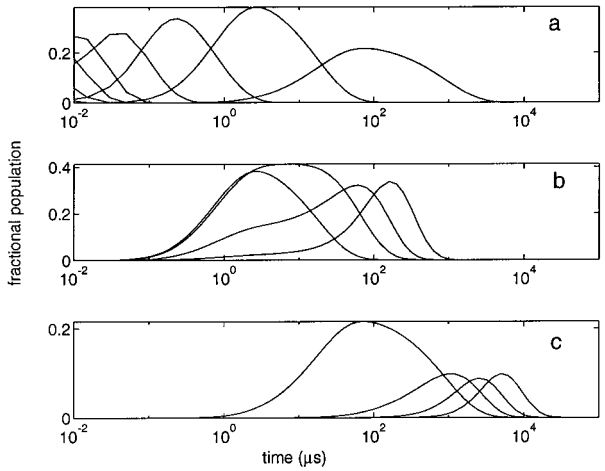

FIGURE 6: Time evolutions of Hb photolysis intermediates calculated from fit of kinetic model in Figure 5 to Soret data in Figure 2. Panels show successive appearance and decay of (a) $A_0^{(4)}$, $A_0^{(3)}$, $A_0^{(2)}$, $A_0^{(1)}$, $A_0^{(0)}$, R'_0, R_0, and T_0; (b) R_0, R_1, R_2, and R_3; and (c) T_0, T_1, T_2, and T_3.

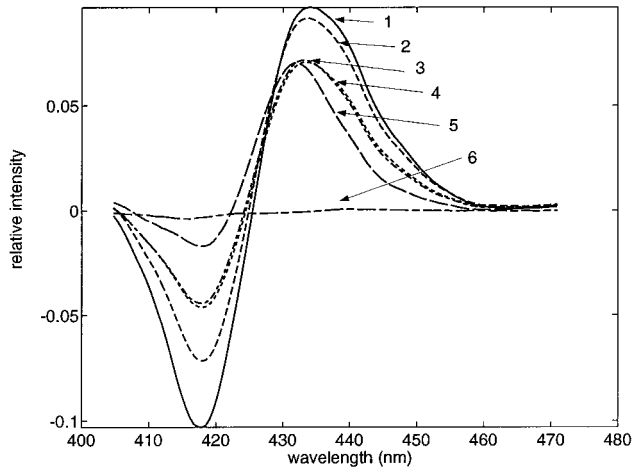

FIGURE 7: The six independent, per heme spectra used to construct intermediate spectra: geminate pair (1, —), ligand escaped (2, - - -), R′ (3, ···), R (4, -·-), T unliganded (5, — - —), and T liganded (6, — — —).

model to the Soret data are plotted logarithmically in Figure 6, which shows the sequential rise and decay of species A_0^4 through T_0, species R_0 through R_3, and species T_0 through T_3 (Figure 5, top row and two right hand columns, respectively). Time-dependent concentrations obtained from the UV data (not shown) are similar. The model obligates each photolyzed heme that escapes geminate recombination to go through the R'_n species before relaxing to R_n, with widely separated time constants for the formation and decay of R_n and R'_n. Thus, both R_n and R'_n reach significant concentrations after photolysis. The small amplitude of the spectral change associated with $R'_n \rightarrow R_n$ (Table 1, relaxation III) then implies very similar spectra for these two species, as seen in Figure 7. Although, the photolysis difference spectra of the two intermediates are similar, the double difference spectrum $R_n - R'_n$ is nevertheless significant in that it strongly resembles the T − R difference spectrum of Perutz et al. (1974a), as shown in Figure 8.

The first observed rate constant, $k_1 = 4.5 \times 10^7\ s^{-1}$, is the sum of rate constants associated with branching between geminate recombination and escape from the heme pocket. In principle, the extent of spectral relaxation accompanying

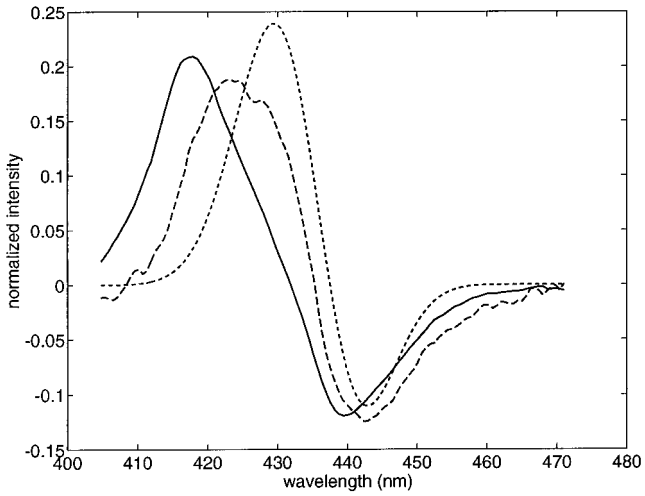

FIGURE 8: Calculated $T_0 - R_0$ (—) and $R - R'$ (- - -) double difference spectra compared with equilibrium T − R (···) spectrum (Perutz et al., 1974a).

ligand escape may be calculated from the model and the value of the branching ratio (geminate yield). However, much of the spectral difference between geminate pair and relaxed pocket in the carboxy region observed in Figure 7 appears to arise from the detection artifact discussed above for the second SVD component. Because of the relatively large uncertainty in the zero of time associated with the ns laser pulse, the high probability of secondary photolysis during the pulse, and detector artifact, we cannot place much confidence in the ligand escape spectral relaxation reported in Figure 7.

The $T_n - R_n$ spectral differences found from the analysis are shown in Figure 8. They resemble the equilibrium T − R spectral difference found by Perutz et al. (1974a), showing a trough near 440 nm and a shoulder near 428 nm, the peak of the T − R difference, but they also contain a large carboxy peak. The latter suggests that the model is mixing some of the CO recombination spectral difference into the $R_n - T_n$ spectral evolution. The branching ratio, Θ, between recombination and the allosteric transition can be calculated from k_4 and the observed R + CO rate constant, k_5, as $\Theta = (k_4 - 4k_5)/k_4 = 0.6$. This is substantially higher than the ratio, 0.15, implied by the six-exponent time constants.

DISCUSSION

We find that at least six observed time constants describe the relaxation of photolyzed HbCO. Five of the six time constants obtained from our data (SVD rank 5) correspond closely with relaxations previously identified in time-resolved absorption studies. Hofrichter et al. (1983) found five relaxations in the Soret absorption bands of human hemoglobin in a study in which CO pressure and extent of photolysis were varied. Their spectral data (SVD rank three) showed that the transient deoxyHb spectrum evolved toward the equilibrium deoxyHb spectrum with relaxation constants to 50 ns, 0.8−1.4 μs, and 20 μs that were assigned to geminate recombination, tertiary structural relaxation within photolyzed subunits, and the R → T globin quaternary change, respectively. Time-resolved absorption studies also find that the overall deoxy−carboxy difference spectrum decays with pseudo-first-order lifetimes of 190 μs and 3.8 ms at 1 atm of CO, corresponding to bimolecular rebinding to the R and T forms, respectively. Heme−heme com-

munication has been found to affect the kinetics of hemoglobin relaxation and ligand recombination at times later than about 1 μs after photodissociation (Jones et al., 1992). The rate constant of the R → T transition, in particular, is expected to depend on the extent of heme ligation, with the rate roughly decreasing by a factor of 2−3 with the addition of each CO (Eaton et al., 1991). (The equilibrium ratio of R to T increases by about 2 orders of magnitude with the addition of each ligand, so that the T → R rate constant is actually more sensitive to ligation than R → T, but the back reaction of T to R is too slow to affect the present study.) The diffusive recombination of CO to R_0 competes with R_0 → T_0, so that the observed R → T rate constant is the sum of rate constants for the quaternary change and recombination.

Several nanosecond time-resolved absorption studies of HbCO photodissociation have previously reported a small amplitude relaxation in the deoxy Soret peak occurring at about 1 μs (Alpert et al., 1979; Lindqvist et al., 1980; Hofrichter et al., 1983). A similar relaxation is observed in isolated α and β chains (Lindqvist et al., 1980), but the much larger magnitude observed in Hb suggests that subunit interactions are important in enhancing the effect of this relaxation on the heme environments in the tetramer. Assigning the nature of this relaxation has proven difficult (Murray et al., 1988). Previous workers noted its spectral similarity to the R → T transition occurring at about 20 μs (Hofrichter et al., 1985), but whereas the extent of the R → T transition is found to depend on the fraction of deligated hemes, no such dependence is observed for the 1-μs process, indicating that the latter process precedes chemically significant communication between hemes after ligand photodissociation (Jones et al., 1992). Nevertheless, photodissociation of CO from heme iron perturbs the spectra of adjacent cobalt-substituted hemes at times as soon as 1 μs in Hb hybrids (Hofrichter et al., 1985). These considerations suggest that heme−heme interactions may be modulated by relaxation III, but they do not significantly affect its kinetic course.

The intriguing similarity between the Soret b-spectra for relaxations III and IV can be seen from the kinetic modeling of intermediate spectra to arise more specifically from the component of relaxation IV associated with the quaternary transition. Although it is common to loosely speak of relaxation IV as the R → T transition, it has long been recognized that this process is actually a composite of the quaternary transition and CO recombination (Hofrichter et al., 1983). In particular, the fastest quaternary relaxation, R_0 → T_0, competes with R_0 + CO → R_1, which proceeds with a rate constant that is four times the per heme rate constant for recombination to R state Hb. We have applied kinetic modeling using the minimal scheme in Figure 5 to isolate and compare the Soret spectral changes associated with R_n' → R_n (relaxation III) and the R_n → T_n component of relaxation IV. The strong spectral similarity between relaxation III and the equilibrium T − R difference spectrum (Perutz et al., 1974a) is significant in that this similarity is found in none of the other relaxation difference spectra except the $T_n - R_n$ difference spectra. We therefore interpret this spectral similarity as evidence that relaxation III involves protein conformational changes that are similar to those involved in the R → T transformation, at least insofar as these affect protein structure near the heme.

There appear to be no previous reports modeling time-resolved absorption spectra with an explicit kinetic model for relaxations after CO photodissociation with which our calculated spectra for Hb intermediates may be compared. Previous studies have recognized that first-order kinetic models connecting a given set of intermediates share the same observed rate constants and have thus analyzed for simple exponential relaxations, equivalent to assuming multiple first-order processes proceeding in parallel. Although we found it necessary to apply many simplifying assumptions in arriving at a tractable, but more realistic, kinetic model of HbCO photolysis, the model presented here appears to be successful in calculating photolysis difference spectra for R_n, R_n', and T_n that give double difference spectra, $R_n - R_n'$ and $T_n - R_n$, that may be validly compared with one another and with the equilibrium T − R spectrum. However, an evident shortcoming of the calculated results is that although the calculated $T_n - R_n$ difference spectra are much more recognizably similar to the equilibrium T − R difference spectrum than is the relaxation IV b-spectrum, the appearance of a carboxy peak in the $T_n - R_n$ difference indicates that the kinetic modeling still mixes in an appreciable amount of the spectral difference associated with ligand recombination. The reason for this mixing is not clear, although the neglect of any back reaction of T_0 to R_0 can be ruled out as a cause given the stability of T_0 relative to R_0. The neglect of R_n → T_n for $n > 0$, on the other hand, is a severe approximation that may lead to incorrect branching between R_0 recombination and conformational switching to T_0 in the current model. Indeed, experimental evidence from partial photolysis measurements indicates that R_1 → T_1 and R_2 → T_2 may make appreciable contributions to relaxation IV (Jones et al., 1992). Inclusion of R_3 → T_3 and the back reactions T_2 → R_2 and T_3 → R_3 also could be expected to significantly affect the calculated branching at R_0 in a more complete kinetic model.

Information from resonance Raman studies is useful in assigning the nature of relaxations II and III. Time-resolved resonance Raman studies of heme core-size frequencies (Terner et al., 1981; Stein et al., 1982; Spiro et al., 1990) find that doming of the heme after ligand photodissociation moves the iron out of the heme plane by as much as 0.5 Å (Fermi, 1975; Perutz et al., 1982) with a time constant of approximately 100 ns, and this process is accordingly assigned to the relaxation II reported here for Soret and near-UV time-resolved absorption. Resonance Raman measurements (Rousseau & Friedman, 1988) also find that the histidine−Fe bond angle tilts from an orientation initially perpendicular to the heme plane with several relaxation rates that are in good agreement with the time constants found from time-resolved absorption. The first relaxation, concomitant with the 100-ns out-of-plane Fe displacement, produces 25%, of total bond angle relaxation within 300 ns of photolysis. Additional histidine relaxation is observed by about 1 μs after photodissociation (Rousseau & Friedman, 1988; Spiro et al., 1990), and the fully relaxed T state deoxy heme position is reached after a final 20-μs relaxation (Rousseau & Friedman, 1988).

Evidence for early changes in protein structure at the $\alpha_1\beta_2$ interface has been found in time-resolved UV resonance Raman studies. Su et al. (1989) found changes in the W3 band of Trp β37 that peaked around 10 μs after photolysis, suggesting that the R → T transition occurs in a stepwise

fashion. Kaminaka et al. (1990) were also able to detect protein structural changes evident in UV resonance Raman spectra as early as 10 μs after photolysis. Rodgers et al. (1992) found a change at about 1 μs in the Trp β37 W17 band that was interpreted in terms of a stepwise quaternary transition, while Rodgers and Spiro (1994) report the approximately 10-μs appearance of the equilibrium T state species as determined from the resonance Raman signal for Trp β37. Most recently, Jayaraman et al. (1995) present UV resonance Raman evidence for the appearance of T-like character at the $\alpha_1\beta_2$ interface with a 0.5-μs time constant. Thus, UV resonance Raman spectra of the interfacial aromatic residues appear to report quaternary conformational changes at the interface that can be associated with relaxation III.

The spectral similarity of relaxation III to both the equilibrium and the photolytic R → T transformation suggests a strong overlap of the relaxation III reaction coordinate with that for the quaternary structure change. In particular, the time-resolved Soret absorption evidence points to an overlap of changes in protein tertiary conformation near the hemes, while the time-resolved UV circular dichroism (Björling et al., 1996) and resonance Raman evidence (Rodgers et al., 1992) suggests an overlap of conformational changes at the dimer−dimer interface.

If relaxation III thus represents the first step in a compound R → T reaction pathway, $R_n' \rightarrow R_n \rightarrow T_n$, then the question arises as to the nature of the kinetic barrier between R_n' and R_n. Although $R_n' \rightarrow R_n$ and $R_n \rightarrow T_n$ apparently proceed along a similar reaction coordinate, several considerations suggest that the extent of progress along this pathway is much smaller for $R_n' \rightarrow R_n$. The small amplitude of the Soret spectral change associated with $R_n' \rightarrow R_n$ indicates a much more modest tertiary change at the heme. The apparent absence of cooperativity in the relaxation III reaction rate suggests that any concomitant changes in dimer−dimer interactions are small and not rate limiting. Another consideration consistent with small quaternary change during $R_n' \rightarrow R_n$ is the lack of evidence for different ligand affinities in R_n' and R_n, although an enhancement in the CO on-rate for R_n' would need to be very dramatic (at least an order of magnitude larger than the enhancement of R_n affinity relative to T_n) to be detectable during the R_n' lifetime. Small changes in tertiary and quaternary structure would also be consistent with the 50-fold faster rate constant for $R_n' \rightarrow R_n$ compared with $R_n \rightarrow T_n$. The latter transformation presumably involves the breaking of numerous dimer−dimer hydrogen bonds and salt bridges as the dimers rotate by 14° relative to one another to form the more extensive nonbonded interactions stabilizing the T state. In the hypothesis of Baldwin and Chothia (1979a), the kinetic barrier to this motion resides in the "switch" region comprising residues 38−44 of the α_1 subunit and residues 97−102 of the β_2 subunit, and particularly in a steric interference to motion of His β97 past Thr α41.

The kinetic barrier between R_n' and R_n apparently arises, therefore, from intra-subunit forces. This free energy barrier would oppose the forces generated by out-of-heme-plane motion of the iron upon ligand photodissociation and their eventual transmission during relaxation III, presumably through the F helix, to the $\alpha_1\beta_2$ interface. Enthalpic contributions to this barrier could arise from steric interference to chain motion as residue side chains come into van der Waals contact. Entropic contributions could be associated with the relatively small number of chain configurations leading to the R_n conformation. Once this free energy barrier to F helix motion is surmounted, the chain is free in this scenario to move toward the rearrangement of interfacial residue conformation detected in near-UV time-resolved resonance Raman and circular dichroism spectroscopy. This rearrangement would be driven by a modest tightening of dimer−dimer contacts, as suggested by resonance Raman evidence for hydrogen bond formation at Trp β37 and Tyr α41 on this time scale (Jayaraman et al., 1995).

Several constraints can now be drawn on possible free energy relationships between R_n', R_n, and T_n and the activation barriers separating these species for a given value of n. Our photolysis data most strongly reflects the behavior of R_0', R_0, and T_0, which are found to be successively more stable. For increasing values of heme ligation, the classic two state model predicts that T_n grows less stable, so that R_2 and T_2 are roughly in equilibrium, and R_4 is several kcal below T_4 in free energy. We have identified the R_0 species in our scenario with the classic two-state R_0 in Figure 1, but can this identification hold through R_4? Apparently it cannot. Because our R_0' species is posited to have the structure of the equilibrium oxy form, we must describe the latter as R_4'. Therefore there must be a reversal in the relative stability of R_n' and R_n on going from $n = 0$ to $n = 4$ (while keeping the $R_n' \rightarrow R_n$ activation barrier and rate constant fixed). A schematic free energy diagram outlining this scenario for the compound $R_n' \rightarrow R_n \rightarrow T_n$ reaction pathway is presented in Figure 9. The main point presented in Figure 9, besides the distinction between two R structures, is the reversal in relative stability of the R forms somewhere between $n = 0$ and $n = 4$.

We briefly consider the possible relationship of the R structures posited here, R_n' and R_n, to known crystal structures for oxyHb. Besides the R quaternary form found in the classic X-ray studies of Perutz (1970) and Baldwin and Chothia (1979), performed on oxyHb crystals obtained under high salt conditions, recent workers have found that a distinct oxyHb crystal structure, denoted Y (Smith et al., 1991; Smith & Simmons, 1994) or R2 (Silva et al., 1992), can be obtained under low salt conditions. Srinivasan and Rose (1994) calculate difference maps between the crystallographic R, R2/Y, and T structures and find that the classic R structure is computationally intermediate (i.e., lies near the linear interpolation) between the R2/Y and T structures. Their calculations show a continuous evolution of structure, particularly in the switch region, along the R2/Y → R → T pathway as measured by surface area buried at the dimer−dimer interface. While they do not calculate energies, they suggest that the R2/Y structure, obtained under more physiologically relevant conditions, may actually be the stable form of oxyHb in physiological solution. It is tempting to speculate therefore that R2/Y and the classic R quaternary structures correspond respectively to the R′ and R species discussed here for the photolysis of HbCO. This speculation is at least consistent with the free energy considerations outlined in Figure 9, with R2/Y being the stable solution structure for fully liganded Hb, and correlates with the progression along the $R_n' \rightarrow R_n \rightarrow T_n$ reaction coordinate inferred from spectral data.

In summary, we have calculated photolysis difference spectra of HbCO photodissociation intermediates from time-

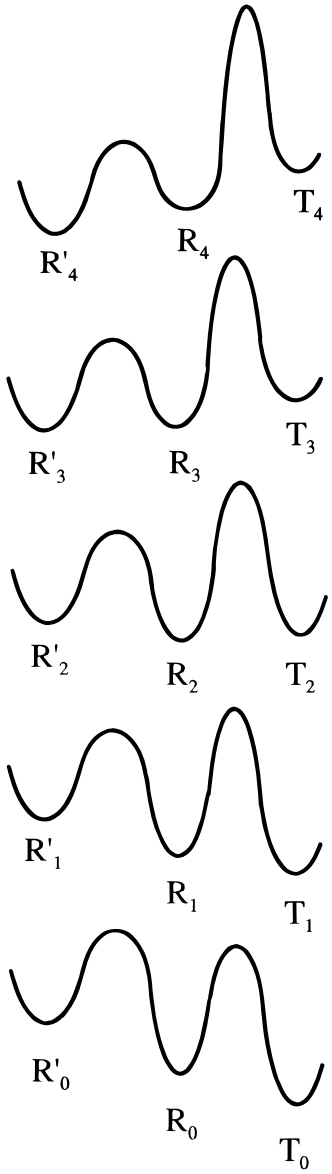

FIGURE 9: Schematic illustration of relative free energy along proposed reaction pathways connecting R'_n, R_n, and T_n.

resolved absorption spectral data, using a microscopic model for intraprotein relaxation and ligand recombination, to better characterize the physical nature of the observed spectral relaxations, particularly the small amplitude spectral relaxation around 1 μs, designated relaxation III. The spectral similarity between relaxation III and the component of the approximately 20-μs process (relaxation IV) corresponding to the quaternary R $\rightarrow$ T transition suggests that relaxation III involves some changes in protein conformation overlapping those in relaxation IV. From this absorption evidence, and from other time-resolved resonance Raman and circular dichroism results, we infer that relaxation III is the first step in a compound R $\rightarrow$ T reaction path. This proposal thus distinguishes two R structures, R′ and R, separated by a thermodynamic barrier with an $R'_n \rightarrow R_n$ activation energy that is independent of n, at least for small values. The R'_n structure, posited to be that of fully ligated HbCO, is probably separated from R_n primarily by tertiary structural forces.

This initial attempt to interpret the kinetic spectroscopy of HbCO photodissociation in terms of a microscopic model has used the minimal number of microscopic rates necessary to account for the six observed relaxation rates extracted from the data. Further elaborations of the kinetic model, such as different rates for α and β chains and the influence of R to T reactions (and back reactions) among singly and higher liganded tetramers, can be expected to yield additional molecular information from analyses of time-resolved spectral data. The large number of additional microscopic rates that can be envisioned for this system suggests that additional exponential relaxation rates should be observable and, indeed, seven exponential fits to time-resolved absorption data have been reported for HbCO photolysis (Hofrichter et al., 1991; Jones et al., 1992). In addition to more refined analyses of kinetic absorption data, along these lines, we are also undertaking time-resolved studies of natural circular dichroism (Björling et al., 1996), optical rotatory dispersion (Shapiro et al., 1995), magnetic circular dichroism (Goldbeck & Kliger, 1993), and magnetic optical rotatory dispersion to further elucidate the nature of intermediates in this system.

ACKNOWLEDGMENT

We thank Drs. James Lewis, Stephan Hug, Thorgeir Thorgeirsson, and Daniel Shapiro for helpful discussions.

REFERENCES

Ackers, G. K., Doyle, M. L., Myers, D., & Daugherty, M. A. (1992) *Science 255*, 54−63.
Alpert, B., El Mohsni, S., Lindqvist, L., & Tfibel, F. (1979) *Chem. Phys. Lett. 64*, 11−16.
Antonini, E., & Brunori, M. (1971) *Hemoglobin and Myoglobin In Their Reactions With Ligands*, Elsevier, New York.
Baldwin, J. M., & Chothea, C (1979a) *J. Mol. Biol. 129*, 158−174.
Baldwin, J. M., & Chothea, C. (1979b) *J. Mol. Biol. 129*, 175−220.
Bellelli, A., & Brunori, M. (1994) *Methods Enzymol. 232*, 56−71.
Björling, S. C., Goldbeck, R. A., Paquette, S. J., Milder, S. J., & Kliger, D. S. (1996) *Biochemistry 35*, 8619−8627.
Brzozowski, A., Derewenda, Z., Dodson, E., Dodson, G., Grabowski, M., Liddington, R., Skarzynski, T., & Vallely, D. (1984) *Nature 307*, 74−76.
Doyle, M. L., Lew, G., Turner, G. J., Rucknagel, D., & Ackers, G. K. (1992) *Proteins 14*, 351−362.
Eaton, W. A., Henry, E. R., & Hofrichter, J. (1991) *Proc. Natl. Acad. Sci. U.S.A. 88*, 4472−4475.
Eckhart, C., & Young, G. (1939) *Bull. Am. Math. Soc. 45*, 118−121.
Fermi, G. (1975) *J. Mol. Biol. 97*, 237−256.
Geraci, G., Parkhurst, L. J., & Gibson, Q. H. (1969) *J. Biol. Chem. 244*, 4664−4667.
Goldbeck, R. A., & Kliger, D. S. (1993) *Methods Enzymol. 226*, 147−177.
Hendler, R. W., & Shrager, R. I. (1994) *J. Biochem. Biophys. Methods 28*, 1−33.
Henry, E. R., & Hofrichter, J. (1991) *Methods Enzymol. 210*, 129−192.
Herzfeld, J., & Stanley, H. E. (1974) *J. Mol. Biol. 82*, 231−265.
Ho, C. (1992) *Adv. Protein Chem. 43*, 153−312.
Hofrichter, J., Sommer, J. H., Henry, E. R., & Eaton, W. A. (1983) *Proc. Natl. Acad. Sci. U.S.A. 80*, 2235−2239.
Hofrichter, J., Henry, E. R., Sommer, J. H., Deutsch, R., Iked-Saito, K., Yonetai, T., & Eaton, W. (1985) *Biochemistry 24*, 2667−2679.
Hofrichter, J., Henry, E. R., Szabo, A., Murray, L. P., Ansari, A., Jones, C. M., Coletta, M., Falcioni, G., Brunori, M., & Eaton, W. A. (1991) *Biochemistry 30*, 6583−6598.
Imai, K. (1982) *Allosteric Effects in Hemoglobin*, Cambridge University Press, Cambridge, England.
Jameson, G. B., & Ibers, J. A. (1994) in *Bioinorganic Chemistry* (Bertini, I., Gray, H. B., Lippard, S. J., & Valentine, J. S., Eds.) pp 167−252, University Science Books, Mill Valley, CA.
Jayaraman, V., Rodgers, K. R., Mukerji, I., & Spiro, T. G. (1995) *Science 269*, 1843−1848.

Jones, C. M., Ansari, A., Henry, W. R., Christoph, G. W., Hofrichter, J., & Eaton, W. A. (1992) *Biochemistry 31*, 6692−6702.
Kaminaka, S., Ogura, T., and Kitagawa, T. (1990) *J. Am. Chem. Soc. 112*, 23−27.
Koshland, D. E., Nemethy, G., & Filmer, D. (1966) *Biochemistry 5*, 365−385.
Lee, A., & Karplus, M. (1983) *Proc. Natl. Acad. Sci. U.S.A. 80*, 7055−7059.
Lewis, J. W., Yee, G. G., & Kliger, D. S. (1987) *Rev. Sci. Instrum. 58*, 939−944.
Lindqvist, L., El Mohsni, S., Tfibel, F., & Alpert, B. (1980) *Nature 288*, 729−730.
Matsukawa, S., Mawatari, K., Yoneyama, Y., & Shimokawa, Y. (1981) *J. Mol. Biol. 150*, 615−621.
Monod, J., Wyman, J., & Changeux, J. P. (1965) *J. Mol. Biol. 12*, 88−118.
Mozzarelli, A., Rivetti, C., Rossi, G. L., Henry, E. R., & Eaton, W. A. (1991) *Nature 351*, 416−419.
Murray, L. P., Hofrichter, J., Henry, E. R., & Eaton, W. A. (1988) *Biophys. Chem. 29*, 63−76.
Perutz, M. F. (1970) *Nature 228*, 734−739.
Perutz, M. F., Ladner, J. E., Simon, S. R., & Ho, C. (1974a) *Biochemistry 13*, 2163−2172.
Perutz, M. F., Heidner, E. J., Ladner, J. E., Beetlestone, J. G., Ho, C., & Slade, E. F. (1974b) *Biochemistry 13*, 2187−2200.
Perutz, M. F., Hasnain, S. S., Duke, P. J., Sessler, J. L., Hahn, J. E. (1982) *Nature 295*, 535−538.
Rodgers, K. R., & Spiro, T. G. (1994) *Science 265*, 1697−1699.
Rodgers, K. R., Su, C., Subramaniam, S., & Spiro, T. G. (1992) *J. Am. Chem. Soc. 114*, 3697−3709.
Rousseau, D. L., & Friedman, J. M. (1988) in *Biological Applications of Raman Spectroscopy, Vol. 3, Resonance Raman Spectra of Heme and Metalloproteins* (Spiro, T. G., Ed.) pp 133−215, Wiley, New York.
Shapiro, D. B., Goldbeck, R. A., Che, D., Esquerra, R. M., Paquette, S. J., & Kliger, D. S. (1995) *Biophys. J. 68*, 326−334.
Shulman, R. G., Hopfield, J. J., & Ogawa, S. (1975) *Q. Rev. Biophys. 8*, 325−420.
Silva, M. M., Rogers, P. H., & Arnone, A. (1992) *J. Biol. Chem. 267*, 17248−17256.
Smith, F. R., & Simmons, K. C. (1994) *Proteins 18*, 295−300.
Smith, F. R., Lattman, E. E., & Carter, C. W. (1991) *Proteins 10*, 81−91.
Spiro, T. G., Smulevich, G., & Su, C. (1990) *Biochemistry 29*, 4497−4508.
Srinivasan, R., & Rose, G. D. (1994) *Proc. Natl. Acad. Sci. U.S.A. 91*, 11113−11117.
Stein, P., Terner, J., & Spiro, T. G. (1982) *J. Phys. Chem. 86*, 168−170.
Su, C., Park, Y. D., Liu, G.-Y., Spiro, T. G. (1989) *J. Am. Chem. Soc. 111*, 3457−3459.
Terner, J., Stong, J. D., Spiro, T. G., Nagumo, M., Nicol, M., & El-Sayed, M. A. (1981) *Proc. Natl. Acad. Sci. U.S.A. 78*, 1313−1317.

BI952248K